12th IFAC International Symposium on
Advanced Control of Chemical Processes
July 14-17, 2024. Toronto, Canada

Model-based dynamical voltage prediction of Zinc-Air cell for piecewise discharge currents

Juan Diego Pineda-Rodriguez * **Cristina Vlad** *
Pedro Rodriguez-Ayerbe * **Woranunt Lao-atiman** **
Sorin Olaru * **Soorathep Kheawhom** **

* *Laboratory of Signals and Systems, Université Paris-Saclay, CNRS, CentraleSupélec, 91190 Gif-sur-Yvette, France (e-mail: {diego.pineda, cristina.vlad, pedro.rodriguez, sorin.olaru}@centralesupelec.fr)*
** *Department of Chemical Engineering, Faculty of Engineering, Chulalongkorn University, Bangkok 10330, Thailand (e-mail: {woranunt.l, soorathep.k}@chula.ac.th)*

Abstract: This paper examines the construction of a parameter-dependent voltage prediction model for a primary Zinc-air cell prototype, focusing on its response time when subjected to multiple step-wise discharge current levels. Laboratory tests have revealed that the dynamic response's time constant varies with discharge current, a phenomenon not adequately addressed in previous analyses. The current research aims to contribute to the existing knowledge by employing a piecewise current profile during a single cell discharge and conducting an identification-type analysis of the relationships between the system's time constants and other state and input variables. The findings presented in this paper hold significant potential for integration into Battery Management Systems and, in the long term, for addressing the inverse problem of State-of-Charge estimation.

Keywords: Parameter identification, Energy storage systems, Battery modelling, Zinc-air cell.

1. INTRODUCTION

There is a growing global awareness of the need to reduce carbon emissions from human activity as their environmental and socio-economical impact becomes louder with the years. To enable this, research is underway in various energy-related fields, such as production, transmission, and distribution. Developing renewable energy sources and technologies is crucial for responding to the increasing energy demand (Qazi et al., 2019), with solar and wind sources sharing the most significant growth potential (Kebede et al., 2022). However, due to their intermittent nature and demand, energy storage is an essential part of the system, as it improves grid efficiency (Olabi et al., 2021), helps with voltage regulation and improves the reliability and quality of the grid (Boicea, 2014).

Batteries are the most commonly used Energy Storage Systems (ESS). In addition to the established technologies, ongoing research explores emerging materials and configurations, aiming to uncover promising alternatives to conventional Li-ion batteries. Metal-air batteries are one of the attempts at safer and more efficient batteries. Multiple scientific areas are mobilized to advance the effective design of batteries, from chemistry engineering to control engineering. Zinc-air and Zinc-air flow batteries are examples of promising technologies thanks to the metal's availability and safety.

From a control perspective, it is crucial to have a suitable model of the cell's behavior to develop a Battery Management System (BMS) that meets the requirements of a particular system. In that regard, studies have approached the cell from its intrinsic properties, such as electrolyte concentration and reaction rates (Lao-Atiman et al., 2019), to characterize its behavior. Although this approach has shown promising prediction results, it is impractical for BMS integration since it requires knowledge of particular physical/chemical properties that are not always available.

In contrast, model-based techniques have been used to analyze the cell's operation, allowing prediction mechanisms to be embedded in BMS and thus to optimize battery life, performance, and safety (Gabbar et al., 2021). The steady-state response of single-cell Zinc-air battery to input currents has been studied in previous research (Olaru et al., 2019) as well as non-linear state space models that use Hammerstein-Wiener approaches to describe the general cell operation (Lao-atiman et al., 2019; Lao-Atiman et al., 2020). These black-box models are useful for predicting the cell's voltage response to multiple input currents with a sufficient charge. However, there is still insufficient exploration of the relationship between the cell's time constant and discharge current, as well as the utilized capacity, particularly as the cell approaches its End-of-Discharge (EoD) voltage, which can cause changes to internal parameters.

The present paper seizes the cell differently and studies the system's time-constant behavior in response to different current levels. The model is evaluated using a grey-box approach, where previous works have already characterized the steady-state behavior (Rodriguez et al., 2023), and a first-order system captures the transient behavior of the cell. A piece-wise discharge current profile is used to analyze the time-constant dependence on the current. The approach discussed here provides a more physically meaningful interpretation of the coefficients within the identified model, allowing for a deeper understanding of the overall system. However, a primary challenge associated with this approach is the inherently sluggish nature of the system. The extended time required to reach steady-state voltage values constrains the number of useful transitions before the cell reaches its EoD state, which impacts data collection for calculating time constants and the subsequent model construction. Furthermore, as the cell approaches near-complete discharge, its transient characteristics undergo a shift in behavior.

With this in mind, the physical operation of the cell and its chemical reaction are described in Section 2.1. Then, the block diagram representation of the system focusing on its transitory is defined in Section 2.2. Section 3 describes the test methodology, assumptions, and the tools used. The model validation and the results analysis are presented in Section 4.

2. SYSTEM DESCRIPTION

2.1 First principles of operation

Zinc-air batteries (ZABs) are a promising type of energy storage system due to their high energy density and specific energy compared to the commercialized lithium-ion batteries (Olabi et al., 2021; Liu et al., 2022). These batteries rely on a redox reaction between oxygen, which acts as a cathode, and zinc, which serves as an anode. Zinc is oxidized, forming zincate ions and releasing electrons to an electrolyte medium, facilitating their transfer between the electrodes. By the end of the reaction, the zincate becomes zinc oxide. The appeal of ZABs lies in the abundance of zinc, making them cheaper, safer, and more stable to operate. Furthermore, using oxygen as a cathode makes them lighter and smaller, reducing the materials needed to build them. Electrolytes can be aqueous or non-aqueous (Olabi et al., 2021). For this study, an aqueous potassium hydroxide (KOH) electrolyte with a concentration of 7M is used. The reaction is as follows:

- Anode:

$$\mathrm{Zn} + 4\mathrm{OH}^- \longleftrightarrow \mathrm{ZnOH}_4^{2-} + 2e^-$$
$$\mathrm{ZnOH}_4^{2-} \longleftrightarrow \mathrm{ZnO} + 2\mathrm{OH}^- + \mathrm{H_2O}$$
$$(E^0 = -1.25 \text{ V vs SHE})$$

- Cathode:

$$\frac{1}{2}\mathrm{O_2} + \mathrm{H_2O} + 2e^- \longleftrightarrow 2\mathrm{OH}^-$$
$$(E^0 = 0.401\text{V vs SHE})$$

where E^0 is the corresponding standard electrode potential versus standard hydrogen electrode (SHE) (Lao-Atiman et al., 2020). The overall reaction is summarized as

$$\mathrm{Zn} + \frac{1}{2}\mathrm{O_2} \longleftrightarrow \mathrm{ZnO}$$

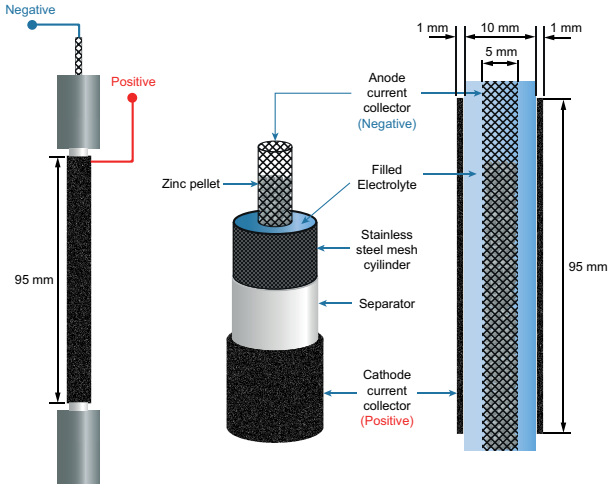

Fig. 1. Structure of the Zinc-air battery (Lao-Atiman et al., 2019).

$$(E^0_{\text{cell}} = 1.65V).$$

The theoretical open-circuit voltage is 1.65 V; however, upon measurement, it exhibits a distribution around 1.4 V for this particular study. The cell consists of a primary (non-rechargeable) prototype developed at Chulalongkorn University in Bangkok, as depicted in Fig. 1.

2.2 Dynamical model description

Complex physical systems require modeling to understand better how they respond to various inputs and internal or external variables. Since the chemical reaction alone does not provide enough information to characterize the macroscopic behavior of these systems, a model of the system's dynamic operation, conceived using abstractions and interconnections to represent the system's behavior, is represented on the block diagram in Fig. 2. This model is based on the following assumptions:

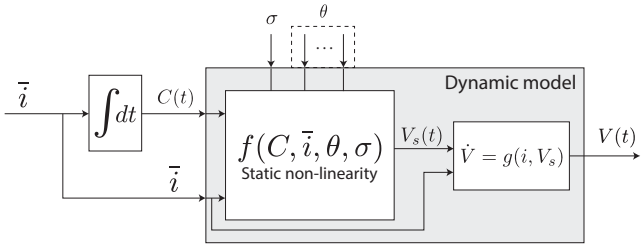

Fig. 2. Block diagram describing the system.

- A static dependency between the output voltage and discharge characteristics, accounted for by a sigmoidal function, denoted as $f(C, i)$, of the form:

$$f(C, i) = \frac{A(C, i)}{1 + \mathrm{e}^{C_1(i)(C - C_{in}(i))}}. \quad (1)$$

The parameters A, C_1, and C_{in} were identified using experimental data, and their values correspond to those reported in (Rodriguez et al., 2023). This function characterizes the cell's internal structure and serves as an indicator of the cell's proximity to complete discharge. In practice, it describes the evolution of the cell's voltage during the discharge period, which changes as a function of the current (due to internal impedances) and the discharged capacity (due to

the nature of the chemical reaction). The sigmoid's inflection point C_{in} marks the approach to full cell discharge.
- A first order differential equation $g(i, V_s)$ portraying the cell's transient dynamics with a current-dependent time constant τ. This parameter is the main element of study in the present work.

The overall system input is a piecewise constant load current $\bar{i}$, which is integrated to obtain the cell's discharged capacity $C(t)$ (also known as discharged coulombs). The output is the cell's voltage $V(t)$, and V_s is the steady-state voltage obtained for $\bar{i}$. Two main variability sources can alter the cell's response to currents. *First*, a parameter vector θ_j that includes variables such as temperature, zinc disposition inside the tube, quality of the electrolyte, etc. Since this study is based on a primary type cell that has to be changed after every discharge, θ is different for every realization j (thus denoted θ_j). For this study, the whole vector θ_j is considered a disturbance affecting the voltage response and is not directly measured. *Second*, despite being a primary battery, the mesh cylinder and the separator are reused for every discharge process; hence, an aging parameter σ embodies the cell's material degradation through time and use. This study does not consider the latter, as the tests were performed with a small time separation. The analysis of this parameter could be included in further studies concerning the cell's State-of-Health (SoH).

This study focuses on finding an appropriate characterization of the time constant evolution as a function of the discharge current that provides a convenient transient response of the cell. Therefore, a method for predicting end-of-discharge points needs to be analyzed in detail.

3. METHODOLOGY

3.1 Data obtention and treatment

To identify the transient response of the cell, it is necessary to draw a consistent and stable load current from it to avoid noise that can affect the measurements. The battery-testing device used is a BTS-4000 from Neware, consisting of an 8-channel device connected to a server. This device allows the programming of the desired reference discharge/charge profiles in the form of constant voltage, current, or power. In the present work, the device is set to a constant current discharge with a 100 ms sampling time (T_s) and a cut-off voltage of 0.01 V. A cycle of constant current steps, from 100 to 900 mA in 100 mA steps as shown in Fig. 3, was drawn. Each step lasts 2.5 minutes, allowing the cell to reach its steady-state voltage. Four-minute rest states are included at the end of each cycle to study the cell's return to the open-circuit voltage. Moreover, the voltage behavior during these states allows us to analyze the evolution of the time constant with respect to the input current and the discharged capacity. It is important to note that the peaks on the voltage response in Fig. 3 result from parasitic phenomena from the test equipment and not from the cell dynamics. This cycle was repeated until the cell's voltage was below the cut-off voltage. After this point, the cell's voltage dynamics change, indicating that it is reaching its end of discharge (or State-of-Charge reaching 0).

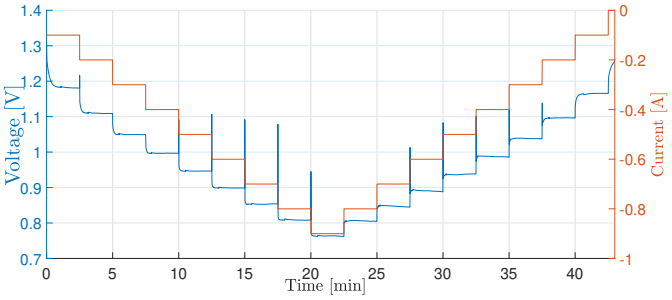

Fig. 3. Output voltage obtained for a pyramid cycle discharge current profile.

The dynamics that start to show nonlinear behavior are not relevant to this study; however, they constitute a compelling continuation for describing the entire system.

3.2 Transitory

The monotone transitory discharge dynamics displayed by the cell can be modeled in terms of a simple first-order system:

$$\dot{V}(t) = -\frac{1}{\tau}V(t) + \frac{1}{\tau}V_s(t). \tag{2}$$

The system's observed time constant (τ) shows a dependence on the input current's amplitude. A set of τ_n is considered, with $n = \{1 \dots 9\}$, where n represents the current step. The aim is to express τ as an explicit function that can describe a continuous evolution of the current, such as $\tau = \hat{\tau}(i)$, and then identify the function $\hat{\tau}(i)$. The time constant was calculated and recorded at every change in the current step to identify this function. To avoid erroneous calculation of τ, the peaks introduced by the testing equipment into the voltage response were post-processed by considering the steady-state value of the voltage one sample before the current change. A least-square curve-fitting is used to identify the function's parameters on the form:

$$\hat{\tau}(i) = ae^{-bi} + c. \tag{3}$$

To validate the model binding the steady-state voltage and the transient response, it was implemented on a Simulink block diagram, depicted in Fig. 4. Due to the nature of the data, the blocks were implemented in their discrete-time form. The first-order discrete-time system is obtained with the Euler discretization and the sampling time T_s:

$$V(k+1) = (1 - \frac{T_s}{\tau})V(k) + \frac{T_s}{\tau}V_s(k). \tag{4}$$

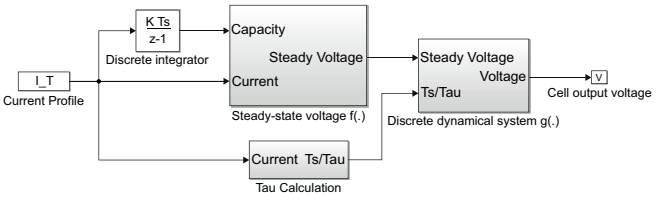

Fig. 4. Simulink block diagram.

4. RESULTS

4.1 Validation of the time constant

The response of a multistep current profile showed that the system's time constant τ varies depending on the

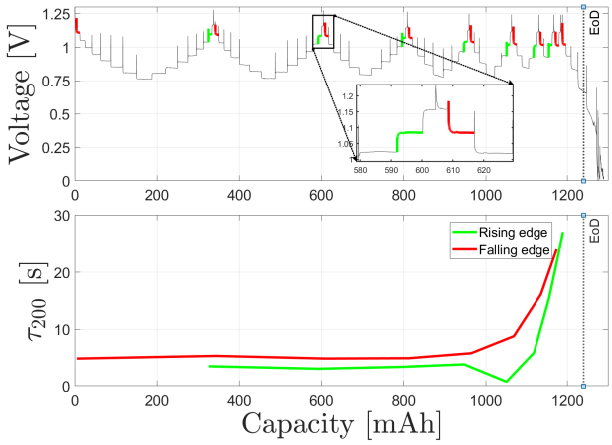

Fig. 5. Estimation voltage profile and τ_{200} values calculated for a 200 mA current setpoint in function of the capacity.

reference current amplitude. However, the values of τ for a given current change around a given current setpoint i_n remain relatively constant as long as the output voltage dependence to capacity is linear (i.e., before the cell's inflection point or cut-off voltage). In contrast, the τ value rises exponentially as the cell approaches its End-of-Discharge (EoD), as portrayed in Fig. 5, meaning a longer time to reach a steady voltage state. The values of $\tau_{\bar{i}}$ slightly change as well depending on the direction of the setpoint change, whether it is a rising or falling edge of discharge current. Consider a reference current i_n; the cell takes longer to reach a steady state voltage when discharged towards a higher current setpoint ($i_{n-1} < i_n$) and less when reducing the reference current ($i_{n-1} > i_n$). This could be caused by the nature of the chemical reaction inertia and available electrons. This paper focuses on the dependency of τ on the discharge current; therefore, the values of the time constant nearing EoD (dependency on the cell's *State-of-Charge*, SoC) were not considered for constructing the function for τ. The observed dependency of τ on the discharged capacity and the direction of the current change constitute starting points for future experiments with richer data.

Three τ subsets were obtained from the current step changes in the estimation profile portrayed in Fig. 7a, to fit a function for τ (equation (3)). The coefficients of the three functions are summarized in Table 1 and consist of:

- The values of τ calculated at the beginning of the discharge test (the first 9 steps going from 100 to 900 mA, therefore, 9 values of τ). The obtained function is called $\tau_f(i)$.
- The average values of τ for step changes around a given nominal current. This means the time constant is recorded every time the cell changes to a current step amplitude i_n. When the test is over, the mean of the τ values for each current i_n is calculated. $\tau_a(i)$ is the fitted function using this data set.
- The median values of τ for step variations around a given nominal current. The median values are then used to fit the function $\tau_m(i)$, as they reduce the influence of outlier values of τ coming from noisy data, in contrast to the mean values.

Table 1. Coefficients of the fitted τ functions

	a	b	c
τ_f	31.28	11.75	1.67
τ_m	26.36	12.01	1.74
τ_a	25.47	13.31	1.84

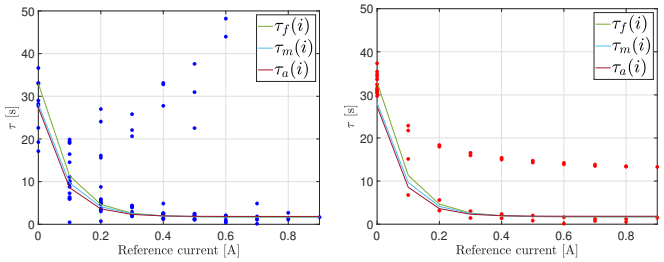

(a) (b)

Fig. 6. τ values calculated for all current setpoints in a. the estimation data and b. the validation set of Fig. 7b.

All the raw τ calculated values can be seen on Fig. 6a along with the fitted functions $\tau_f(i)$, $\tau_a(i)$, and $\tau_m(i)$. This figure includes the values of time constants computed close to the EoD. These particular values are shifted vertically to higher values. Once the functions $\hat{\tau}(i)$ are constructed, they can be analysed on different validation datasets. It is the case with respect to the profile in Fig. 6b, which exhibits an important shift according to a different profile of the discharge steps.

To assess the fitted $\hat{\tau}(i)$ functions, a comparison has been made using two performance indices, according to the equations (5) and (6).

$$J_a = \frac{\sum_k (\tau_k - \hat{\tau}(i))^2}{\sum_k (\tau_k - \bar{\tau})^2} < 1 \tag{5}$$

$$J_l = \frac{\sum_k (\tau_k - \hat{\tau}(i))^2}{\sum_k (\tau_k - \check{\tau}(i))^2} > 1 \tag{6}$$

where τ_k is every calculated τ for a given setpoint current i, $\hat{\tau}(i)$ is the respective $\tau(i)$ function being analyzed (τ_f, τ_a or τ_m), $\bar{\tau}$ is the mean value of **all** the calculated time constants (independently of the current) and $\check{\tau}(i)$ is the mean value of the time constant for a given reference current i. The performance index values for each fitted function related to each data set are resumed in Table 2.

Table 2. Performance indices for each fitted function

	J_a	J_l
$\tau_f(i)$	0.978	1.34
$\tau_m(i)$	0.964	1.32
$\tau_a(i)$	0.974	1.33

According to Table 2, the closer J_a is to 0, the better the fit of the function, whilst the closer J_l is to 1, the more accurate the function is for predicting a value of τ. With this in mind, the function fitted with the median values $\tau_m(i)$ is the best at predicting the behavior of the system's time constant. However, despite the fitting

performances, the validation of the transitory model needs to be extended to complex input signal excitation. A comparison is provided between the simulation model in Fig. 4 and the effective cell data as follows:

- The curve on Fig. 7a is the set used for the dynamical model parameter identification (estimation set).
- The profile in Fig. 7b starts with a similar profile to the one in Fig. 7a. However, another section is included to study the rest periods on the cell, which allowed to calculate the time constant for the system returning to the open-circuit voltage ($i = 0$). It also includes longer steps at the end to study the influence of longer periods under discharge, which showed no effect on the time constant's value.
- Fig. 7c aims to study the cell's response to stronger changes in the discharge current (i.e., larger step amplitudes Δi). No obvious effect has been observed on the value of τ for higher variations Δi.

The validation needs key indicators for the quality of identification. The RMS error and a third performance index given by equation (7) were calculated for each one of the curves in Fig. 7, as shown in Table 3.

$$J = \frac{\sum_t (y(t) - \hat{y}_{\hat{\tau}}(t))^2}{\sum_t (y(t) - \hat{y}_{\bar{\tau}}(t))^2} < 1 \tag{7}$$

Table 3. RMSE and J values for datasets

		τ_f	τ_m	τ_a
Estimation set (Fig. 7a)	RMSE	0.042	0.042	0.042
	J	0.938	0.938	0.936
Fig. 7b	RMSE	0.090	0.088	0.087
	J	0.984	0.934	0.927
Fig. 7c	RMSE	0.037	0.035	0.035
	J	0.946	0.871	0.861
Fig. 7d	RMSE	0.072	0.072	0.071
	J	0.966	0.966	0.965
Fig. 8	RMSE	0.014	0.014	0.014
	J	0.971	0.912	0.889

The profiles portrayed in Fig. 7 show a good approximation of the system's transient response. The slight differences between the actual steady-state voltage values and those predicted by the identified model come from parameter variation across experiments (θ_n). These variations are not considered as the parameters of the static nonlinear function $f(.)$ were identified from the estimation set shown in Fig. 7a. This can be more clearly seen in Fig. 7d, where a large offset is observed between the estimated and measured outputs. Fig. 8 shows a preliminary correction of the estimated output by rectifying the cell's open-circuit voltage considered in the function $f(.)$, which improves the prediction's RMSE and J values. The values of J in Table 3 being inferior to 1, and Fig. 9, underlines the interest in using a current-varying time constant compared to a unique, constant value for τ. Nonetheless, it reveals in the same time that a steady-state error between the model and the real values influences the performance index J (as this latter relies on this "steady" error). Further improvement can be brought to the model with parameter adjustment (online or offline) for fine-tuning the cell steady-state voltage estimation, which constitutes an interesting analysis for future developments.

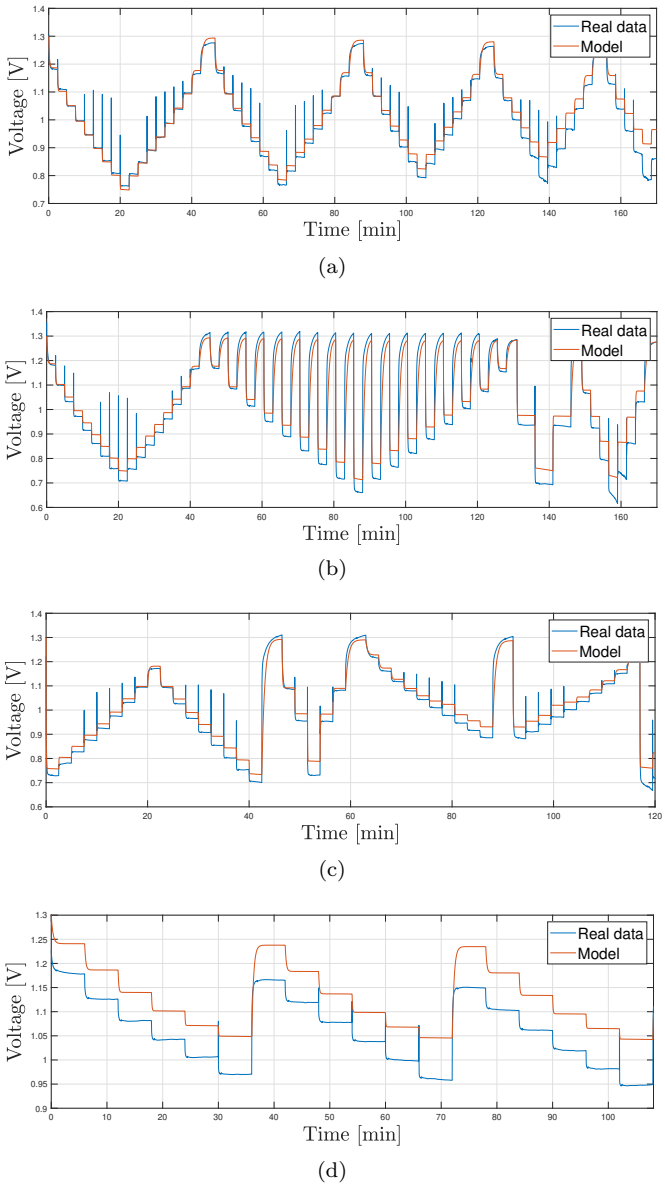

Fig. 7. Simulation and experimental results to multiple profiles.

Regarding the time constant estimation, Table 2 points $\tau_m(i)$ as the best option for predicting this aggregate value along the evolution of the discharge current. Yet, the RMSE and J values in Table 3 put light on $\tau_a(i)$ as a better candidate for estimation when using the $\hat{\tau}$ function in the global model presented in Fig. 4. Nonetheless, there is a significant setback on this estimation method, considering that obtaining a $\hat{\tau}(i)$ function based on its average values (or even its median values) along the entire discharge profile implies performing a complete discharge. Such an extensive test is impractical in Battery Management Systems (BMS). A possible approach to this question in future studies could be an estimation along a defined window so that a complete discharge is unnecessary. This is where the $\hat{\tau}$ functions are particularly interesting. Finally, let us recall that including the dependency on the cell's SoC in the analysis may also improve the prediction's accuracy and extensive discharges need to be further performed in order to put the current analysis in a statistical perspective.

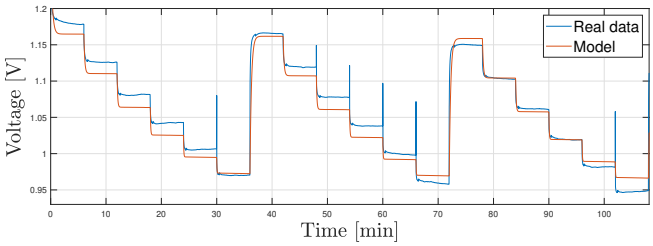

Fig. 8. Adjusted cell voltage prediction.

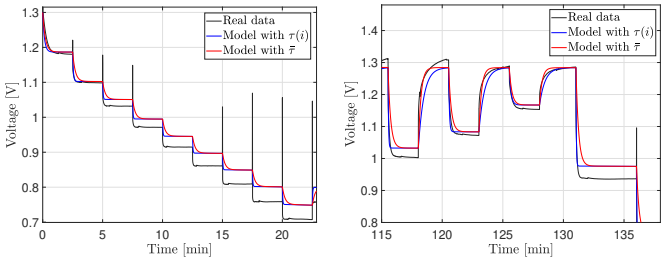

Fig. 9. Focus on two areas of the validation set of Fig. 7b showing the comparison between the model using a varying $\tau(i)$ and a constant $\bar{\tau}$.

4.2 Time constant measurement for EoD anticipation

In addition to providing a more accurate model whilst including the transient response of the system, the time constant's value monitoring may prove itself very useful for anticipating the cell's End-of-Discharge (EoD). As seen in Fig. 5, the τ values calculated for current changes slightly before the voltage drop point cease to have a constant tendency. A τ value threshold can be defined within a Battery Management System (BMS) to detect when the cell is approaching depletion. Further studies with richer data on the transitory behavior of the cell can assist in defining this threshold, by deepening the analysis of the capacity dependency of the time constant. This will aid in enhancing the EoD prediction by a BMS.

5. CONCLUSIONS

Studying the transitory behavior of the zinc-air cell is important to build a reliable model. This work aims to have a deeper insight into the dynamic behavior of a particular construction of a primary zinc-air cell. To do this, an in-depth analysis of the system's time constant, which had yet to be previously conducted, is carried out. Real-time measurements allowed to contribute in this regard by complementing the model for the steady-state behavior with an expression for the dynamical performance of the cell with a current-dependent time constant. This was achieved by using the piecewise constant discharge currents that provided information on the variability of the time constant using a single cell. The results obtained in this work will serve as a basis for future procedures, enabling richer data to improve the parameter fitting process. Also, two main continuations might be of interest to go further with this topic. First, a deeper examination of the time constant's dependence on cell degradation or SoH and State-of-Charge, as it might constitute an insightful method for estimating them. Second, an adaptive procedure could be integrated into the system to adjust the parameters of the model based on the different realizations of the cell as well as changes in external or internal parameters that are not taken into account, such as temperature or electrolyte concentration, to give an example.

REFERENCES

Boicea, V.A. (2014). Energy storage technologies: The past and the present. *Proceedings of the IEEE*, 102(11), 1777–1794.

Gabbar, H., Othman, A., and Abdussami, M. (2021). Review of battery management systems (BMS) development and industrial standards. *Technologies*, 9(2), 28.

Kebede, A.A., Kalogiannis, T., Mierlo, J.V., and Berecibar, M. (2022). A comprehensive review of stationary energy storage devices for large scale renewable energy sources grid integration. *Renewable and Sustainable Energy Reviews*, 159, 112213.

Lao-Atiman, W., Bumroongsil, K., Arpornwichanop, A., Bumroongsakulsawat, P., Olaru, S., and Kheawhom, S. (2019). Model-based analysis of an integrated zinc-air flow battery/zinc electrolyzer system. *Frontiers in Energy Research*, 7, 15.

Lao-atiman, W., Kheawhom, S., and Olaru, S. (2019). Zinc-air battery dynamics' identification using transfer functions and hammerstein-wiener models. In *2019 23rd International Conference on System Theory, Control and Computing (ICSTCC)*, 332–337. IEEE.

Lao-Atiman, W., Olaru, S., Arpornwichanop, A., and Kheawhom, S. (2019). Discharge performance and dynamic behavior of refuellable zinc-air battery. *Scientific data*, 6(1), 1–7.

Lao-Atiman, W., Olaru, S., Diop, S., Skogestad, S., Arpornwichanop, A., Cheacharoen, R., and Kheawhom, S. (2020). Linear parameter-varying model for a refuellable zinc–air battery. *Royal Society Open Science*, 7(12), 201107.

Liu, J.N., Zhao, C.X., Wang, J., Ren, D., Li, B.Q., and Zhang, Q. (2022). A brief history of zinc–air batteries: 140 years of epic adventures. *Energy Environ. Sci.*, 15, 4542–4553.

Olabi, A.G., Sayed, E.T., Wilberforce, T., Jamal, A., Alami, A.H., Elsaid, K., Rahman, S.M.A., Shah, S.K., and Abdelkareem, M.A. (2021). Metal-air batteries—a review. *Energies*, 14(21), 7373.

Olaru, S., Golovkina, A., Lao-atiman, W., and Kheawhom, S. (2019). A mathematical model for dynamic operation of zinc-air battery cells. *IFAC-PapersOnLine*, 52(17), 66–71.

Qazi, A., Hussain, F., Rahim, N.A., Hardaker, G., Alghazzawi, D., Shaban, K., and Haruna, K. (2019). Towards sustainable energy: A systematic review of renewable energy sources, technologies, and public opinions. *IEEE Access*, 7, 63837–63851.

Rodriguez, J.D.P., Olaru, S., Vlad, C., Rodriguez-Ayerbe, P., Lao-atiman, W., and Kheawhom, S. (2023). Model-based voltage prediction for a zinc-air cell subject to piecewise constant discharge currents. In *2023 9th International Conference on Control, Decision and Information Technologies (CoDIT)*. IEEE.